

New gravity-capillary waves at low speeds

Part 1: Linear geometries

PHILIPPE H. TRINH^{1,2} AND S. JONATHAN CHAPMAN²

¹Program in Applied and Computational Mathematics, Princeton University,
Washington Road, Princeton, NJ, 08544, USA

²Oxford Centre for Industrial and Applied Mathematics, Mathematical Institute,
24-29 St. Giles', Oxford, Oxfordshire, OX1 3LB, UK

(Received — and in revised form —)

When traditional linearised theory is used to study gravity-capillary waves produced by flow past an obstruction, the geometry of the object is assumed to be small in one or several of its dimensions. In order to preserve the nonlinear nature of the obstruction, asymptotic expansions in the low-Froude or low-Bond number limits can be derived, but here, the solutions invariably predict a waveless surface at every order. This is because the waves are in fact, exponentially small, and thus *beyond-all-orders* of regular asymptotics; their formation is a consequence of the divergence of the asymptotic series and the associated Stokes Phenomenon.

By applying techniques in exponential asymptotics to this problem, we have discovered the existence of new classes of gravity-capillary waves, from which the usual linear solutions form but a special case. In this paper, we present the initial theory for deriving these waves through a study of gravity-capillary flow over a linearised step; this will be done using two approaches: in the first, we derive the surface waves using the standard method of Fourier transforms; in the second, we derive the same result using exponential asymptotics. Ultimately, these two methods give the same result, but conceptually, they offer different insights into the study of the low-Froude, low-Bond number problem.

Key Words: surface gravity waves, capillary waves, wave-structure interactions

1. Introduction

Our interest in the gravity-capillary problem lies with the complicated scenario of waves induced by interactions with objects in a stream. Here, the first significant theory was proposed by Lord Rayleigh (1883), whose chief source of inspiration had been the earlier experiments of Scott Russell (1844) and Thomson (1871). As Lord Rayleigh (1883) himself explains:

When a small obstacle, such as a fishing line, is [...] held stationary in moving water, the surface is covered with a beautiful wave-pattern, fixed relatively to the obstacle. On the up-stream side the wavelength is short, and, as Thomson has shown, the force governing the vibrations is principally cohesion. On the down-stream side the waves are longer, and are governed principally by gravity.

Rayleigh supposed that the fluid could be assumed to be two-dimensional, inviscid, incompressible, and irrotational, and that the effects of the fishing line could be approximated

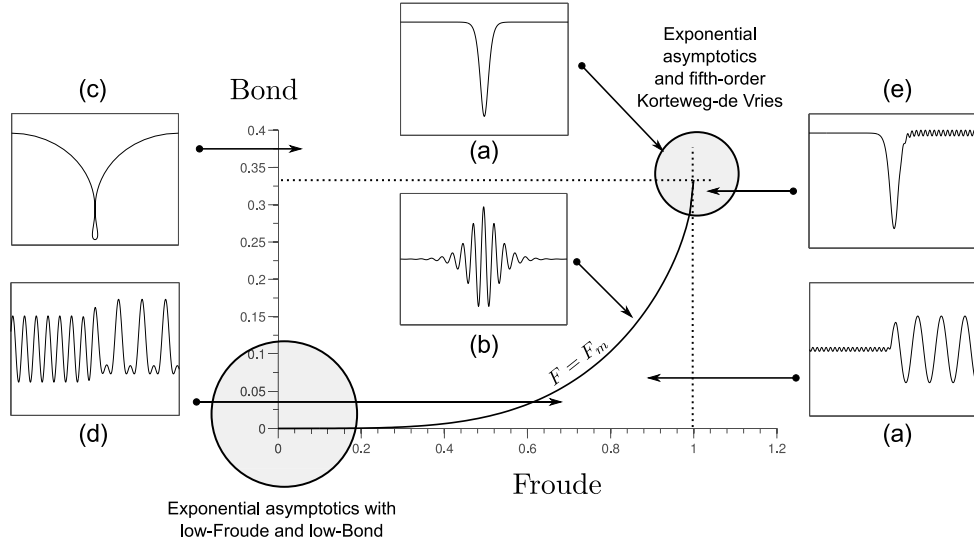


FIGURE 1. Many types of gravity-capillary waves can be found when studying steady finite-depth flows subject to a disturbance. Possible solutions include profiles with (a) trapped bubbles, (b) solitary waves, (c) generalised solitary waves, (d) capillary waves upstream and gravity waves downstream, (e) localised wavepackets, and (f) Wilton ripples. The circled region in the lower-left, corresponding to low-Froude and low-Bond flows has been largely ignored and we aim to study this asymptotic limit.

by the application of a small pressure distribution to a single point on the free-surface (as might be produced by a small jet of air). Then, by linearising for small-amplitude waves and for a weakly-applied pressure distribution, the method of Fourier transforms produces an approximation of the upstream capillary waves and downstream gravity waves. As Rayleigh remarked, the theory is particularly successful in predicting that those particular wave patterns can only exist when the speed of the stream is somewhat faster than 23 centimetres per second.

Since Lord Rayleigh's seminal work, however, mathematical analyses of the general gravity-capillary problem have led to the realisation that, while the study of gravity-only or capillary-only flows are themselves rich in difficulties, the combination of both effects presents a much more formidable challenge. For the theory of finite-depth gravity-capillary waves, the Froude number F , representing the ratio between inertial and gravitational forces, and the Bond number B , representing the ratio between gravitational and surface tension forces, are the two crucial parameters in the problem. In Figure 1, we have illustrated a few of the different kinds of solutions that might be expected when studying even the simplest problems incorporating both effects. Generally, we can expect qualitatively similar types of behaviours even for different types of geometries (finite or infinite depth, perturbed by a submerged object or a pressure distribution, *etc.*). Thus, we will continue to refer to Figure 1, even for the case of Rayleigh's solution (for example), which is only technically applicable for infinite-depth flows.

The figure contains several key regions of interest that are primarily separated by the curve $F = F_m$, the line $B = 1/3$, and the line $F = 1$; we will address these bifurcations later in the text, and they are also described in Appendix A. Notice that if we begin with Rayleigh's fishing line problem, then solutions like the one in (d) may appear, but only in the region below the critical *dispersion curve* of $F = F_m$. In addition to Rayleigh's work, Forbes (1983) and Grandison & Vanden-Broeck (2006) have also studied

this problem of capillary-upstream, gravity-downstream waves, but for flows over a semi-circular obstruction. Within the region below $F = F_m$, it is also possible to find solutions (f) exhibiting the so-called *Wilton Ripples* phenomenon (Wilton 1915); solutions with these secondary ripples have been computed numerically for the waves generated by a moving pressure distribution (Vanden-Broeck 2002), and have also been seen in nature (Schooley 1960).

If the Froude number is now held fixed, and the Bond number is increased, then as we approach the critical dispersion curve, the solution set bifurcates. In particular, Rayleigh's result is singular as this curve is approached, and the system may bifurcate into one of many possible solutions in the form of envelope solitary waves (e), where an appropriate model is the forced Nonlinear Schrödinger Equation. If the Bond number is increased further and past $B = 1/3$, then the solutions take the form of classical solitary waves (b) and can then be approximated by a forced Korteweg-de Vries Equation. Within all these regions, there is occasionally the possibility of non-uniqueness, and a single point in (F, B) space often does correspond to multiple solutions, for which only one represents a perturbation from the uniform flow; for example, solutions can exhibit trapped bubbles (a), representing a perturbation from Crapper's (1957) exact solution of the unforced pure-capillary problem. These issues have been investigated for the case of flow induced by an applied pressure distribution by many authors, including Vanden-Broeck & Dias (1992), Dias & Vanden-Broeck (1993), Dias *et al.* (1996), and Maleewong *et al.* (2005*a,b*).

Finally, the historically controversial region just to the right of the line $F = 1$ separates subcritical and supercritical flows, and exists as a warning sign to those who remain unaware of the importance of exponentially small terms in singular problems. The earliest numerical simulations of this region, computed from the full nonlinear equations, were performed by Hunter & Vanden-Broeck (1983). What they discovered was that when the Bond number is greater than $1/3$, the solution resembles the classical depression solitary wave of (b); but if the Bond number is instead less than $1/3$, the numerical solutions are bedeviled by small-scale oscillations near the tails (c). These dimpled solutions could not be explained at the time, and their significance was quickly glossed over.

However, in the years that followed, a series of papers by Hunter & Scheurle (1988), Pomeau *et al.* (1988), Beale (1991), and Sun (1991) established the notion of nonlocal (or generalised) solitary waves—essentially, a solitary wave coupled with exponentially small oscillations near the tails. Near the point $F = 1$, $B = 1/3$, the water waves are governed by the fifth-order Korteweg-de Vries Equation, for which recent standardised techniques in exponential asymptotics can be applied (Grimshaw 2010; Trinh 2010). Indeed such ripples have been observed for the related case of internal gravity waves Akylas & Grimshaw (1992). The unique history and ultimately, the resolution of the fifth-order Korteweg-de Vries Equation is well documented and described in Boyd (1998).

What do we plan to accomplish?

There are two areas that still require much work: what is the nature of gravity-capillary waves over more general topographies that *cannot* be considered small (such as over a large step in a channel or past any full-bodied obstruction) and in particular, what analytical and numerical work can be done in the regime where the Froude and Bond numbers tend to zero.

The crucial idea is that in the zero-Froude and zero-Bond solution, the free-surface is replaced by a rigid wall, with the full geometry of the obstruction preserved in the solution. Thus, asymptotic approximations for low-Froude and low-Bond numbers allow us to directly relate the generation of waves to the shape of the obstruction. This is in marked contrast to more traditional linear approximations which depend on an asymptotic limit

of small obstructions. The difficulty in the low-Froude, low-Bond limits, however, is that it represents a singular limit. At ever-decreasing Froude and Bond numbers, we would still expect waves to appear on the free-surface, but it is easy to check that the approximation at every single order in the asymptotic hierarchy yields a waveless solution. The waves are, in fact, exponentially small and thus *beyond-all-orders* of traditional asymptotics; in the context of gravity-only flows, this has been termed the *Low-Speed Paradox*, first mentioned by Ogilvie (1968).

In this paper, we will study the problem of flow over a rectangular step, but rather than performing the full low-Froude, low-Bond analysis for $\mathcal{O}(1)$ geometries, we first linearise for asymptotically small steps. The mathematical formulation is presented in §3, and from here, the analysis can proceed in two equivalent ways. In §4, we will regard the Froude and Bond numbers as fixed and $\mathcal{O}(1)$, and solve using Fourier transforms, after which we take $F, B \rightarrow 0$. This is to be contrasted to §5, where we will take $F, B \rightarrow 0$ immediately after the initial linearisation, and then make use of exponential asymptotics.

Our goals are twofold. First, we wish to compare and contrast the method of Fourier transforms with the method of exponential asymptotics. Do concepts like the Stokes Phenomenon and optimal truncation become more transparent using one approach over the other? Second, we wish to show how exponential asymptotics can be applied to the simpler linearised equations of the small-step problem. In the continuation of this paper (Part 2), we will work with the full nonlinear equations; this first excursion, then, provides a smooth transition to the more advanced techniques that underly the subsequent work. Similar ideas of comparing and contrasting the Fourier and exponential-asymptotics approach were used by Mortimer (2004) and Chapman & Mortimer (2005) in the study of partial differential equations.

2. Illustration of the general methodology

Before proceeding to the mathematical analysis, however, we shall describe the key ideas which underly the study to come.

Consider flow over a rectangular step in a channel. From the introduction, we know that for subcritical ($F < 1$) flows linearised theory predicts two regions of interest. In Region I below the critical dispersion curve of Figure 7, we expect flows with capillary waves upstream and gravity waves downstream, while in Region II above the dispersion curve, we expect localised solitary waves. As we will show in §4, the key difference between Type I and II solutions is the kind of residue contributions that are collected in the Fourier inversion process: Region I solutions have four real residues (representing two real wavenumbers) while Region II solutions have four complex residues. However, this phenomenon can also be interpreted using exponential asymptotics, and we now give a taste of the underlying ideas of §5.

When the free surface, described by the fluid speed $q(\phi)$, and streamline angle $\theta(\phi)$, as functions of the potential ϕ , is expanded into an asymptotic series in powers of the Froude and Bond numbers, then we find that the expansions of q and θ are waveless to every order. The exponentially small waves on the free-surface must instead be interpreted as arising from the *Stokes Phenomenon*, by which the coefficient of a subdominant exponential in an asymptotic expansion appears to change discontinuously as a so-called *Stokes line* is crossed. These concepts are connected to the divergence of the asymptotic expansions, and are reviewed in, for example, the works of Dingle (1973) and Boyd (1998, 1999).

Of course, the velocity $qe^{-i\theta}$ is entirely well-behaved on the free surface, but its analytic continuation contains a singularity corresponding to the sharp rise in the step. It is this singularity that causes the asymptotic series to diverge, and is the origin of the Stokes

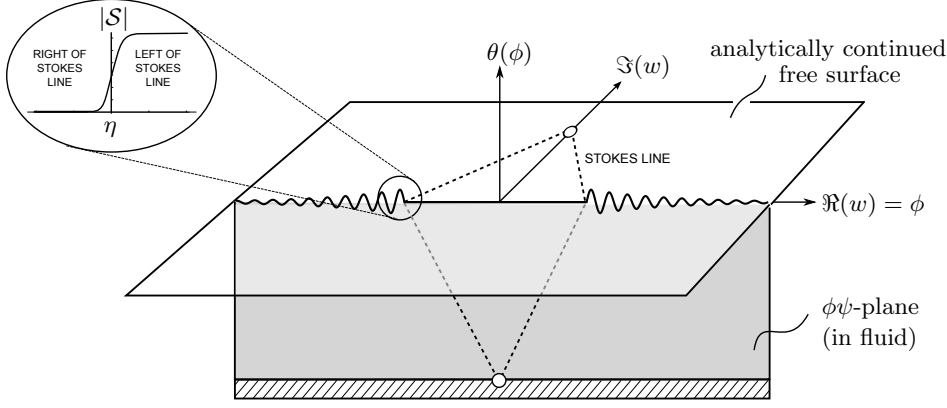


FIGURE 2. The *physical* solutions of interest is θ , the angle of the free-surface as a function of the potential $\phi \in \mathbb{R}$. The free-surface can be analytically continued, producing the perpendicular plane, $\phi = w \in \mathbb{C}$. This complex plane shares a correspondence with the physical $\phi\psi$ -plane (darkly shaded). Singularities are shown as circles and Stokes lines are dashed. Singularities and Stokes lines in the lower complex w -plane are not illustrated.

lines. To study this issue, we complexify the free-surface, sending $\phi \mapsto \bar{\phi} + i\bar{\psi} = \bar{w} \in \mathbb{C}$ and $qe^{-i\theta} \mapsto \bar{q}e^{-i\bar{\theta}} = d\bar{w}/d\bar{z} \in \mathbb{C}$. This is represented by the perpendicular plane (out of the page) in Figure 2. However, because of the nature of complex variables, we may continue to identify these new complexified variables, \bar{w} and $d\bar{w}/d\bar{z}$, with the usual quantities of w (the complex potential) and dw/dz (the complex velocity).

In Figure 2, the darkly shaded plane depicts the *physical* $\phi\psi$ -plane—that is, the plane where fluid lies above the solid boundary, and where there is a single singularity due to the small step. In this work, we may speak of the *corner of the step generating a wave*, but we are actually referring to the singularity in the analytic continuation, identifiable with the step, rather than the step itself.

Once we have located these singularities, then we can expect Stokes lines (dashed in Figure 2) to emerge from each one, across which the Stokes Phenomenon necessitates the switching-on of exponentially small waves (whose amplitudes scales like $|S|$ in Figure 2). Afterwards, by the process of optimal truncation and Stokes smoothing, we can explicitly derive the form of the waves that switch on. Our work in this paper is an extension of the methods developed by Chapman & Vanden-Broeck (2002) for capillary waves, and Chapman & Vanden-Broeck (2006) for gravity waves. These studies are themselves based on the procedure of optimal truncation and Stokes smoothing, as described in Olde Daalhuis *et al.* (1995) and Chapman *et al.* (1998). In fact, the rectangular step in this paper is chosen for its simplicity; the exponential asymptotics theory will be later applied (in Part 2) to flows over more general nonlinear geometries (see also related work by Trinh *et al.* (2011) and Lustri *et al.* (2012)).

It is important to note that this technique of optimal truncation and Stokes smoothing is presented here in preparation for the nonlinear analysis of Part 2. Indeed, for the simpler problem of Part 1, it is an equally valid approach to apply a WKB analysis to the linearised equation and search for solutions of the form $Qe^{-\chi/\epsilon}$. In the nonlinear variant, the same idea allows us to determine the argument of the exponentials, χ , but not the constant (Stokes) multipliers, Q . Finding these Stokes multipliers is the key difficulty of nonlinear problem, and one method is to use the exponential asymptotics presented here.

However, the methodology we use is not the only such approach for studying exponen-

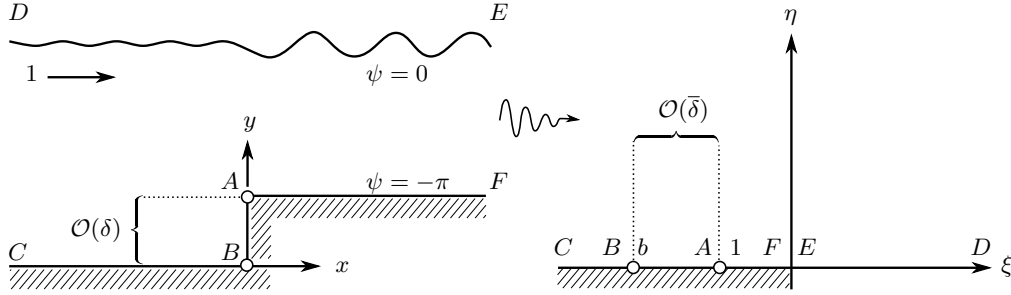


FIGURE 3. The flow in the physical xy -plane (left) is first mapped to the potential $w = \phi + i\psi$ plane, then again mapped to the upper half $\zeta = \xi + i\eta$ plane (right) using $\zeta = e^{-w}$. Later, the analysis will proceed by assuming that the height of the step is small.

tially phenomena. Indeed, there exists a substantial community that uses, for example, Borel summation and for which the relevant waves originate from singularities in the Borel plane. We refer readers to the tutorials and reviews by Boyd (1998, Chap. 4), Olde Daalhuis (1999), Costin (2008), Grimshaw (2010) and the references therein.

3. Mathematical formulation

Consider steady two-dimensional potential flow of an incompressible fluid over a rectangular step in a channel (Figure 3). Far upstream, the flow is uniform with constant velocity U and the height of the channel is L . We first non-dimensionalise the velocity with U and the length with L/π . Then, if the fluid velocity is $\mathbf{u} = (u, v) = \nabla\phi$, the potential satisfies Laplace's equation,

$$\nabla^2\phi = 0. \quad (3.1)$$

On all boundaries, we have the kinematic condition,

$$\frac{\partial\phi}{\partial n} = 0, \quad (3.2)$$

and on the free surface, Bernoulli's equation gives

$$\frac{F^2}{2} (|\nabla\phi|^2 - 1) + y = -B\kappa, \quad (3.3)$$

where $F = U/\sqrt{gL}$ is the Froude number defined for gravitational constant g ; $B = \sigma/(\rho g L^2)$ is the Bond number defined according to the surface tension parameter σ and density ρ ; and κ is the curvature, defined to be positive if the center of curvature lies in the fluid region.

We then define the complex potential by $w = \phi + i\psi$, where ψ is the streamfunction, and conformally map the flow from the physical plane to the strip between $\psi = -\pi$ and $\psi = 0$. A second transformation with $w \mapsto \zeta = \xi + i\eta = e^{-w}$ is then used to map the potential plane to the upper-half ζ -plane. The stagnation and corner points of the step are mapped to $\zeta = -1$ and $\zeta = -b$, respectively, and we can prescribe the step by $y = \delta f(x) = \delta H(x)$ where $H(x)$ is the Heaviside function and $\delta \ll 1$. These physical and ζ -planes are shown in Figure 3.

The flow can now be handled more easily by formulating the problem in terms of the hodograph variables, $\log(dw/dz) = \log q - i\theta$, where q is the speed of the flow and θ is the angle the streamlines make with the x -axis. Then by Cauchy's Theorem, it can be

shown that

$$\log q = -\frac{1}{\pi} \int_{-\infty}^{\infty} \frac{\theta(\xi')}{\xi' - \xi} d\xi'. \quad (3.4)$$

Reposing the potential problem in terms of this integral formulation is a standard technique—see for example, King & Bloor (1987, 1990) and Tuck (1991) for further descriptions. Bernoulli's equation (3.3) can also be transformed into a more convenient form by differentiating with respect to the arclength parameter s (increasing in the flow direction), and using

$$\frac{d}{ds} = \frac{d\phi}{ds} \frac{d}{d\phi} = q \frac{d}{d\phi}.$$

Then after rearranging, Bernoulli's equation becomes

$$F^2 \left[q^2 \frac{dq}{d\phi} \right] - B \left[q^2 \frac{d^2\theta}{d\phi^2} + q \frac{dq}{d\phi} \frac{d\theta}{d\phi} \right] = -\sin \theta. \quad (3.5)$$

Note that in the usual treatment of linearised flow in a channel (*cf.* Lamb 1932 and King & Bloor 1987, 1990) the problem is typically nondimensionalised so that the channel depth is 1. Our decision to nondimensionalise with a depth of π is instead consistent with the choice of Chapman & Vanden-Broeck (2006).

4. Classical linearised theory for small steps

Linearised solutions for flow over a slight bottom topography have been treated for the case of gravity waves in the classic text of Lamb (1932) as well in King & Bloor (1987, 1990). For the case of gravity-capillary waves, Forbes (1983) performed the analysis for flow over a semi-circular obstruction (using the Joukowski map), but surprisingly, a similar analysis does not seem to have been done for the case of flow over a step.

First, so as to distinguish the free-surface and boundary, we use the following notation: if $\xi > 0$ and hence we are positioned on the free-surface, then we let $\xi = e^{-\phi}$ and $\theta(\xi) = \theta_f(\phi)$, where ϕ varies between ∞ and $-\infty$; otherwise, if $\xi < 0$ and we are positioned on the channel bottom, then we let $\xi = -e^{-\phi}$ and $\theta(\xi) = \theta_b(\phi)$, where now ϕ varies between $-\infty$ and ∞ . The boundary integral (3.4) can first be written as

$$\begin{aligned} -\frac{1}{\pi} \int_{-\infty}^{\infty} \frac{\theta(\xi')}{\xi' - \xi} d\xi' &= -\frac{1}{\pi} \left[\int_{-\infty}^{\infty} \frac{\theta_f(s)}{1 - e^{-(\phi-s)}} ds - \int_{-\infty}^{\infty} \frac{\theta_b(t)}{1 + e^{-(\phi-t)}} dt \right] \\ &\equiv P_f(\phi) \end{aligned}$$

with $\phi \in (-\infty, \infty)$. $P_f(\phi)$ can then be written as a sum of convolutions

$$P_f(\phi) = -\frac{1}{\pi} \left[(\theta_f * k_+)(\phi) - (\theta_b * k_-)(\phi) \right], \quad (4.1)$$

where

$$k_{\pm}(\sigma) = \frac{1}{1 \mp e^{-\sigma}}, \quad (4.2)$$

and the convolution product is defined by

$$(g * h)(\phi) \equiv \int_{-\infty}^{\infty} g(s) \cdot h(\phi - s) ds. \quad (4.3)$$

To linearise θ for small steps, we set

$$\theta = \delta\theta^{(1)} + \delta^2\theta^{(2)} + \dots \quad (4.4)$$

so that for $\xi > 0$ and along the free-surface, $q(\xi) = \exp\{P_f(\phi)\} = 1 + \mathcal{O}(\delta)$ from the expression in (3.4). Then at $\mathcal{O}(\delta)$ we get:

$$\bar{\theta}_b^{(1)} = f'(\phi), \quad (4.5)$$

$$F^2 \frac{dP_f^{(1)}}{d\phi} - B \frac{d^2\theta_f^{(1)}}{d\phi^2} = -\theta_f^{(1)}. \quad (4.6)$$

Here and henceforth, primes denote differentiation in ϕ (or later, w). Note that (4.5) can be obtained using the relations $\tan \theta_b = f'(x(\phi))$ and $dx/d\phi = \cos \theta/q$, applied along the channel bottom. Finally, (4.6) can be written as

$$-\frac{F^2}{\pi} \frac{d}{d\phi} \left[(\theta * k_+)(\phi) - (f' * k_-)(\phi) \right] - B \frac{d^2\theta}{d\phi^2} = -\theta. \quad (4.7)$$

In this last equation, we have replaced the notation of $\theta_f^{(1)}$ with θ , so long as it remains clear that we are only interested in the first approximation, evaluated along the free-surface.

4.1. Fourier integrals

We will define the Fourier transform of a function, $f(x)$ as

$$\mathcal{F}[f] \equiv \int_{-\infty}^{\infty} f(x) e^{-ikx} dx.$$

Taking the transform of eqn (4.7) gives

$$-\frac{F^2}{\pi}(-ik) \left[\mathcal{F}[\theta] \mathcal{F}[k_+] - \mathcal{F}[f'] \mathcal{F}[k_-] \right] - B(ik)^2 \mathcal{F}[\theta] = -\mathcal{F}[\theta],$$

and we can use the fact that

$$\mathcal{F}[k_+] = -\frac{\pi i}{\tanh \pi k} \quad \text{and} \quad \mathcal{F}[k_-] = -\frac{\pi i}{\sinh \pi k}, \quad (4.8)$$

and rearrange to get

$$\mathcal{F}[\theta] = \frac{kF^2}{kF^2 \cosh \pi k - \sinh \pi k(Bk^2 + 1)} \int_{-\infty}^{\infty} f'(t) e^{-ikt} dt. \quad (4.9)$$

Inversion then gives the form of the free-surface:

$$\theta = \frac{F^2}{2\pi} \int_{-\infty}^{\infty} \frac{k}{g(k) \cosh \pi k} \left[\int_{-\infty}^{\infty} f'(t) e^{ik(t-\phi)} dt \right] dk, \quad (4.10)$$

where

$$g(k) = kF^2 - \tanh(\pi k)(Bk^2 + 1) \quad (4.11)$$

is the dispersion relation and we will go on to define the inversion contour more specifically in the next section. The different root arrangements of the dispersion relation and their relationships with the various solutions mentioned in the introduction is expounded in Appendix A, but briefly, there are two types of poles: the first type lies entirely on the imaginary axis and affects the free surface primarily near the origin $\phi = 0$. Setting $k = \pm\beta_0, \pm\beta_1, \dots$, where $\beta_i \in \mathbb{R}$, we see that these poles are given by solving the equation:

$$\frac{\tan(\pi\beta_n)}{\beta_n} = \frac{F^2}{1 - B\beta_n^2}, \quad \text{for } n = 1, 2, 3, \dots \quad (4.12)$$

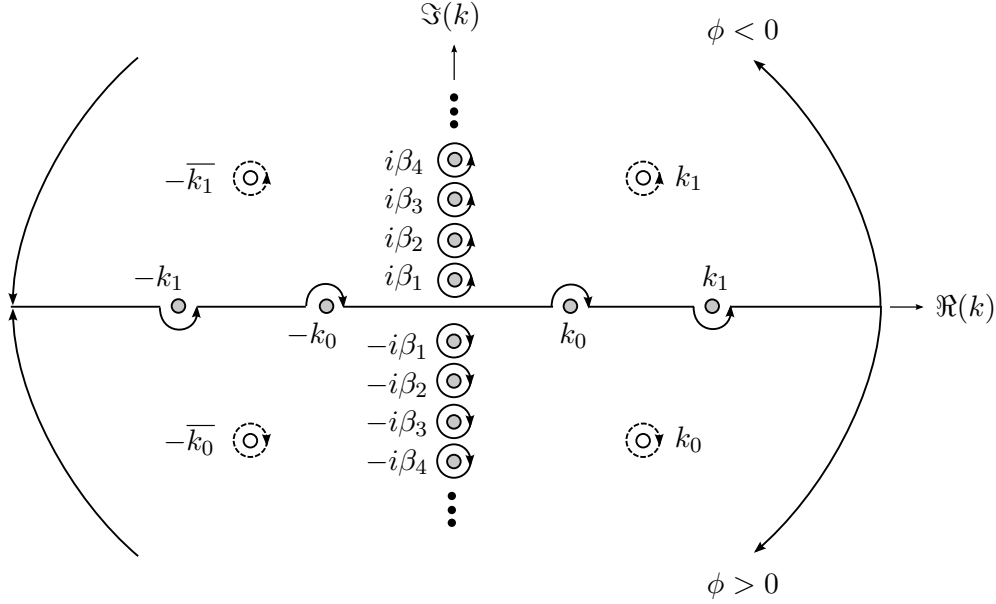


FIGURE 4. When there are four real wavenumbers, the Fourier inversion of eqn (4.13) is done so that for $\phi > 0$, the gravity residues ($k = \pm k_0$) are collected, whereas for $\phi < 0$, the capillary residues ($k = \pm k_1$) are collected. If there are four complex wavenumbers, then the residues in the upper and lower-half plane are similarly collected, in the orientation prescribed by the dotted lines.

and where $\beta_0 = 0$. The second type of pole corresponds to the wavenumbers of the gravity-capillary waves; if we let $k = \pm k_0, \pm k_1$ be these wavenumbers and order them according to their behaviours as determined in Region I (of Figure 7), then $\pm k_0$ corresponds to gravity waves and $\pm k_1$ to capillary waves, with $0 < k_0 < k_1$. However, if the Froude and Bond numbers are chosen to lie in Region II (of Figure 7), then the four residues will be entirely complex, and we identify the poles in the lower-half plane with k_0 and $\overline{-k_0}$, and the poles in the upper-half plane with k_1 and $\overline{-k_1}$. The reasons for this will become clear in the next section.

4.2. Fourier inversion

At this point, we will now substitute the expression $f(t) = H(t)$ for the geometry of the step into (4.10), giving

$$\theta = \frac{F^2}{2\pi} \int_{-\infty}^{\infty} \frac{k e^{-ik\phi}}{g(k) \cosh(\pi k)} dk. \quad (4.13)$$

First, let us perform the Fourier inversion for solutions in Region I, so with four real wavenumbers; the contour is illustrated in Figure 4.

The definition of the integral in (4.13) suffers from the presence of the four poles along the real axis, and this is a symptom of the unnatural and idealised steady-state problem [*c.f.* Stoker (1957, p.174) and Debnath (1994, p.44)]. We must re-define the integration contour along the real k -axis, taking in account the correct radiation conditions far upstream and far downstream from the disturbance. Suppose that $\phi > 0$: in this case, we deform the contour into the lower-half k -plane, where the integrand tends to zero as $k \rightarrow -i\infty$. In the limit that $\phi \rightarrow \infty$, we want to preserve only gravity waves, and so we only collect the residues from $k = \pm k_0$. Similarly, if $\phi < 0$, then we still deform into the

upper-half k -plane, but the path is chosen so that the residues $k = \pm k_1$ are collected as $\phi \rightarrow -\infty$.

With this in mind, we may write the Fourier integral (4.13) as

$$\theta = \frac{F^2}{2\pi} \int_{-\infty}^{\infty} \frac{G(k)}{g(k)} dk = \frac{F^2}{2\pi} \begin{cases} \left[\oint_{+k_0} + \oint_{-\overline{k_0}} + \sum_{n=1}^{\infty} \oint_{-i\beta_n} \right] \frac{G(k)}{g(k)} dk & \phi > 0 \\ \left[\oint_{+k_1} + \oint_{-\overline{k_1}} + \sum_{n=1}^{\infty} \oint_{+i\beta_n} \right] \frac{G(k)}{g(k)} dk & \phi < 0, \end{cases} \quad (4.14)$$

where $G(k) = ke^{-ik\phi}/\cosh(\pi k)$ and the integral-shorthand represents contour integrals around the indicated poles. Note that we have also included the residue contribution from $k = i\beta_0 = 0$ since this is simply zero. Rather than performing the separate cases for the upstream and downstream solutions, let us write $k = k^*$ for either k_0 or k_1 , and where we thus require $\Re(k^*) > 0$ and $\Im(k^*) \geq 0$ for $\phi \leq 0$.

Away from the critical curves and between regions in Figure 7, the poles are simple roots of $g(k)$, so the upstream and downstream solutions can be written as

$$\begin{aligned} \theta_{\pm} &= \frac{F^2}{2\pi} \left[\pm 2\pi i \left\{ \frac{G(k^*)}{g'(k^*)} + \frac{G(-\overline{k^*})}{g'(-\overline{k^*})} \right\} \pm 2\pi i \sum_{n=1}^{\infty} \frac{G(\pm i\beta_n)}{g'(\pm i\beta_n)} \right], \\ &= F^2 i \left[\pm 2i\Im \left\{ \frac{G(k^*)}{g'(k^*)} \right\} \pm \sum_{n=0}^{\infty} \frac{G(\pm i\beta_n)}{g'(\pm i\beta_n)} \right], \end{aligned} \quad (4.15)$$

where we have used the properties of g and G to conclude that $\frac{G(-\overline{k})}{g(-\overline{k})} = -\frac{\overline{G(k)}}{g(k)}$. From (4.15), the solution can then be expressed as

$$\begin{aligned} \theta_{\pm} &= F^2 \left[\frac{\pm 2|k^*|e^{\Im(k^*)\phi}}{|g'(k^*)\cosh(\pi k^*)|} \right] \sin \left(\Re(k^*)\phi - \text{Arg}(k^*) + \text{Arg}[g'(k^*)\cosh(\pi k^*)] \right) \\ &\quad - F^2 \sum_{n=1}^{\infty} \left[\frac{\beta_n}{\cos(\pi\beta_n)g'(i\beta_n)} \right] e^{-\beta_n|\phi|}, \end{aligned} \quad (4.16)$$

and the \pm signs in (4.16) are associated with $\phi \leq 0$, respectively. Again, recall that for gravity ($-$) waves, we set $k^* = k_0$ while for capillary ($+$) waves, we set $k^* = k_1$. Note that from expression (4.16) for θ , the (re-scaled) free-surface can then be computed from

$$y \sim \delta \int^x \theta(s) ds,$$

and moreover, in the limit that $\phi \rightarrow \pm\infty$, the contributions from $k = \mp i\beta_n$ of (4.16) tend to zero, leaving only the contributions from the residues at $k = \pm k_0, \pm k_1$.

4.3. Taking the Low-Froude and low-Bond limits

The key result of the previous section, eqn (4.16), provides the form of the gravity-capillary waves over a small step. However, we are more interested in the nature of this approximation as the Froude and Bond numbers tend to zero, so we let $F = \beta\epsilon$ and $B = \beta\tau\epsilon^2$, where $\epsilon \ll 1$. This particular scaling for F and B is chosen so that a power of ϵ is associated with each derivative of the dependent variables of (3.3)—thus ϵ for the gradient $\nabla\phi$, and ϵ^2 for the curvature κ . The reason for this choice will become clear later when we perform the exponential asymptotic analysis.

With this choice for the Froude and Bond numbers, a balance of terms in eqn (4.11)

tells us that $k = \mathcal{O}(1/\epsilon)$. Since $\tanh(\pi k) \sim 1$ for $\Re(k) > 0$, we can write the dispersion relation (4.11) as

$$\beta\tau(\epsilon k)^2 - \beta(\epsilon k) + 1 \sim 0,$$

where we only consider the roots with $\Re(k) > 0$. Then we have the fact that

$$k_{\pm} \sim \frac{D_{\pm}}{\epsilon}, \quad (4.17)$$

where D_{\pm} is defined by

$$D_{\pm} \equiv \frac{1 \pm \sqrt{\Delta}}{2\tau}, \quad (4.18)$$

with Δ defined by

$$\Delta \equiv 1 - \frac{4\tau}{\beta}. \quad (4.19)$$

The negative sign of eqn (4.17) corresponds to gravity waves ($k_- = k_0$) and the positive sign to capillary waves ($k_+ = k_1$), and the condition that both wavenumbers are real is equivalent to $\Delta > 0$ or $\tau < \beta/4$. In fact, this also indicates that the critical dispersion curve $F = F_m$ in Figure 1 and Figure 7 tends to the curve $B = F^2/4$ as $F \rightarrow 0$. Now, using k_{\pm} (4.17) and D_{\pm} (4.18) in $g'(k)$ (4.11), we can show that

$$g'(k_{\pm}) \sim \mp \beta \epsilon \sqrt{\Delta}, \quad (4.20)$$

and also that

$$\cosh(\pi k_{\pm}) \sim \cosh\left(-\frac{\pi}{\epsilon} D_{\pm}\right) = \frac{1}{2} \left(e^{-\pi D_{\pm}/\epsilon} + e^{\pi D_{\pm}/\epsilon} \right) \sim \frac{e^{\pi D_{\pm}/\epsilon}}{2}. \quad (4.21)$$

Returning to the form of the linear solution (4.16), notice that the terms in the infinite sum are exponentially small as $|\phi| \rightarrow \infty$. Certainly for the case where $\Im(k^*) = 0$, the contribution from the sinusoidal waves remains in the far field, but it is still unclear at the moment what role the infinite sum plays, particularly when $\phi = \mathcal{O}(1)$. This will be clarified in the exponential asymptotics to come. We now use (4.17)–(4.21), and isolate the wave component of the solution (4.16) in the low-Froude, low-Bond limit. As $|\phi| \rightarrow \infty$, the amplitude of the waves (in θ) is shown to be

$$\text{Amplitude of } \theta_{\text{exp}} \sim \frac{4\delta}{\epsilon} \left| \frac{D_{\pm}}{\sqrt{\Delta}} \right| \exp \left[-\frac{\pi \Re(D_{\pm})}{\epsilon} - \frac{|\Im(D_{\pm})\phi|}{\epsilon} \right] \quad (4.22)$$

where we have multiplied the first-order approximation by δ . Notice that in this final result, we have inserted additional absolute-value signs for $\Im(D_{\pm})\phi = \pm \sqrt{\Delta}\phi$. This is in order to dispel the ambiguity of the sign of $\sqrt{\Delta}$ when $\Delta < 0$ and in order to enforce the condition that the waves decay as $\phi \rightarrow \pm\infty$ [indeed, recall the restrictions of k^* in (4.15) and (4.16)].

This completes our determination of the gravity-capillary waves, and we now move on to retrieve a similar result using exponential asymptotics.

5. Exponential asymptotics

In the classical linearisation method of the previous section, we derived the small-step formula (4.16) for $F, B = \mathcal{O}(1)$, only to afterwards take the low-Froude, low-Bond limits. In the method of exponential asymptotics, we will instead take the $F, B \rightarrow 0$ limit *immediately* after the initial linearisation.

As explained in our overview of the methodology, we want to complexify the free boundary variables (ξ, ϕ, q, θ) , which is simply equivalent to replacing the variables by their (2D) complex analogue. Analytically continuing the boundary integral (3.4) into the upper-half ξ -plane gives,

$$\log q - i\theta = -\frac{1}{\pi} \int_{-\infty}^0 \frac{\theta(\xi')}{\xi' - \zeta} d\xi' + \mathcal{H}\theta(\zeta), \quad (5.1)$$

where we have relabeled $\xi \mapsto \zeta$ and \mathcal{H} denotes a Hilbert transform operator on the free-surface, $\xi' \geq 0$:

$$\mathcal{H}\theta(\zeta) = -\frac{1}{\pi} \int_0^{\infty} \frac{\theta(\xi')}{\xi' - \zeta} d\xi'. \quad (5.2)$$

Complexifying the dynamic condition (3.5) also gives

$$\beta\epsilon \left[q^2 \frac{dq}{dw} \right] - \beta\tau\epsilon^2 \left[q^2 \frac{d^2\theta}{dw^2} + q \frac{dq}{dw} \frac{d\theta}{dw} \right] = -\sin\theta, \quad (5.3)$$

with a relabeling of $\phi \mapsto w$, and where we have used the scalings for the Froude and Bond numbers given in §4.3. The expressions in (5.1)–(5.3) then provide an equation for the complexified free-surface, and this was illustrated using the perpendicular plane in Figure 2. At the end of the analysis, we must also remember to add any solutions from analytic continuation into the *lower*-half ζ -plane.

Assuming that the step is small, and letting $b = 1 + \bar{\delta}$, where $\bar{\delta} \ll 1$, then linearising around the uniform stream gives

$$q = 1 + \bar{\delta}q' + \mathcal{O}(\bar{\delta}^2) \quad \text{and} \quad \theta = \bar{\delta}\theta' + \mathcal{O}(\bar{\delta}^2). \quad (5.4)$$

Then (5.1) gives to leading order in $\bar{\delta}$ (dropping primes)

$$q - i\theta = \frac{1}{2(\zeta + 1)} + \mathcal{H}\theta(\zeta). \quad (5.5)$$

The dynamic condition in (3.5) gives to leading order in $\bar{\delta}$ (also dropping primes)

$$\beta\epsilon \frac{dq}{dw} - \beta\tau\epsilon^2 \frac{d^2\theta}{dw^2} = -\theta,$$

and using the fact that

$$\frac{d}{dw} = -\zeta \frac{d}{d\zeta}, \quad \frac{d^2}{dw^2} = \zeta \frac{d}{d\zeta} + \zeta^2 \frac{d^2}{d\zeta^2},$$

the linearised dynamic condition becomes

$$\beta\epsilon\zeta \frac{dq}{d\zeta} + \beta\tau\epsilon^2 \left[\zeta^2 \frac{d^2\theta}{d\zeta^2} + \zeta \frac{d\theta}{d\zeta} \right] = \theta. \quad (5.6)$$

5.1. Outer problem

We first write the solutions of eqns (5.5) and (5.6) as a regular asymptotic expansion:

$$\theta \sim \sum_{n=0}^{\infty} \epsilon^n \theta_n \quad \text{and} \quad q \sim \sum_{n=0}^{\infty} \epsilon^n q_n, \quad (5.7)$$

which gives at leading order,

$$\theta_0 = 0, \quad (5.8)$$

$$q_0 = \frac{1}{2(\zeta + 1)}, \quad (5.9)$$

while at $\mathcal{O}(\epsilon^n)$ for $n \geq 1$, we have

$$q_n = i\theta_n + \mathcal{H}[\theta_n(\zeta)] \quad (5.10)$$

$$\beta\zeta \frac{dq_{n-1}}{d\zeta} + \beta\tau \left[\zeta^2 \frac{d^2\theta_{n-2}}{d\zeta^2} + \zeta \frac{d\theta_{n-2}}{d\zeta} \right] = \theta_n. \quad (5.11)$$

Now the leading-order solution q_0 in (5.9) has a singularity in the analytic continuation of the free-surface, $\zeta = -1$, which corresponds to the corner of the linearised step. But we see by eqns (5.10)–(5.11) that at each subsequent order, q_n is determined by the first and second derivatives of q_{n-1} and q_{n-2} , respectively. Thus, each subsequent order must add to the power of the early singularity, so that in the limit that $n \rightarrow \infty$, the effect of this early singularity dominates the behaviour of the late-order terms; q_n , then, will diverge like a factorial over power:

$$q_n \sim \frac{Q\Gamma(n+\gamma)}{\chi^{n+\gamma}}, \quad (5.12)$$

with γ constant, Q and χ as functions of ζ , and with $\chi(-1) = 0$; of course, the same process leads to a similar expression for θ_n :

$$\theta_n \sim \frac{\Theta\Gamma(n+\gamma)}{\chi^{n+\gamma}}. \quad (5.13)$$

At this point, we can profit from yet another simplification: as $n \rightarrow \infty$, and when ζ is taken near the Stokes line (which we will soon derive), the integral in (5.10) is found to be exponentially subdominant to the other terms of the same equation. Essentially, this occurs because $|\chi|$ is smallest near the singularity, $\zeta = -1$, and grows along the Stokes line as it tends towards the free-surface, upon which the integral is evaluated. This simplification was used in Chapman & Vanden-Broeck (2002, 2006), was discussed in detail for the more interesting case of ship waves in Trinh *et al.* (2011), and was also rigorously justified in the context of the Saffman-Taylor viscous fingering problem by Xie & Tanveer (2003); in any case, the assumption can simply be checked *a posteriori* after obtaining the correct form of χ . From (5.10) then, we have

$$q_n \sim i\theta_n, \quad (5.14)$$

valid as $n \rightarrow \infty$. Using this simplification, the $\mathcal{O}(\epsilon^n)$ terms are then given by (5.11), with

$$\beta\zeta \frac{dq_{n-1}}{d\zeta} - \beta\tau i \left[\zeta^2 \frac{d^2q_{n-2}}{d\zeta^2} + \zeta \frac{dq_{n-2}}{d\zeta} \right] \sim -iq_n. \quad (5.15)$$

Substitution of the ansatz in (5.12) into (5.15) gives to leading order as $n \rightarrow \infty$:

$$(\beta\tau i\zeta^2) \left(\frac{d\chi}{d\zeta} \right)^2 + (\beta\zeta) \frac{d\chi}{d\zeta} - i = 0, \quad (5.16)$$

or

$$\frac{d\chi}{d\zeta} = -i \left[\frac{\beta \pm \sqrt{\beta^2 - 4\beta\tau}}{2\beta\tau} \right] \left(-\frac{1}{\zeta} \right) \implies \frac{d\chi}{d\zeta} = iD_{\pm} \left(\frac{1}{\zeta} \right), \quad (5.17)$$

with D_{\pm} as in (4.18). Requiring that $\chi(-1) = 0$, we then have

$$\chi = iD_{\pm} \log(-\zeta). \quad (5.18)$$

(For convenience, we shall sometimes drop the subscript notation of \pm where it is not

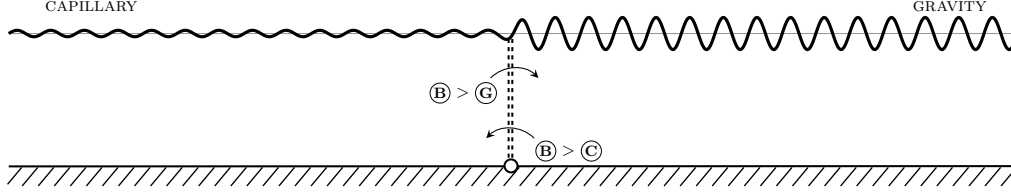


FIGURE 5. In Region I with $\Delta > 0$, both capillary and gravity Stokes lines emerge from $w = -i\pi$ and intersect the origin. Across this point, we expect a gravity wave to switch-on downstream and a capillary wave to switch-on upstream.

relevant). Proceeding to next order in (5.15), we also have

$$\frac{dQ}{d\zeta} \left[\beta\zeta i - 2\beta\tau\zeta^2 \frac{d\chi}{d\zeta} \right] = Q \left[\beta\tau\zeta^2 \frac{d^2\chi}{d\zeta^2} + \beta\tau\zeta \frac{d\chi}{d\zeta} \right]$$

and substituting the equation for χ in (5.18) zeros the right-hand side of the above expression; therefore $Q = \text{constant} = \Lambda$. Finally, to determine the constant γ , we note that in order to match the the leading order solution in eqn (5.9) with the ansatz of eqn (5.12), we need $\gamma = 1$.

Before we go on to discuss the implications of these late-order terms, let us inspect the singulant, χ . From Dingle (1973), we know that Stokes lines must emerge from the singularity at $\zeta = -1$, and are prescribed by locations where successive terms in the expansions of θ and q have the same phase, *i.e.* where

$$\Im(\chi) = 0 \quad \text{and} \quad \Re(\chi) \geq 0.$$

From this, we can verify that in the lower-half complex potential plane (which we identify with points in physical space), the Stokes lines are given by the curves $w = \mu(s) \in \mathbb{C}$ with

$$\mu(s) = \begin{cases} si & \text{if } \Delta > 0 \text{ and for } s \in [-\pi, 0] \\ s + i \left[\frac{\Re(D_{\pm})}{\Im(D_{\pm})} s - \pi \right] & \text{if } \Delta < 0 \text{ and for } |s| \in \left[0, \pi \frac{\Im(D_{\pm})}{\Re(D_{\pm})} \right]. \end{cases} \quad (5.19)$$

Consider the case that $\Delta > 0$. As shown in Figure 5, both the capillary and gravity Stokes lines coalesce along the imaginary ψ axis, and we would thus expect for waves to switch-on as the free-surface is analytically continued across the origin—gravity waves downstream and capillary waves upstream. This transition is denoted either by $\textcircled{B} > \textcircled{C}$ or $\textcircled{B} > \textcircled{G}$, describing the action of the base solution (5.7) switching on a capillary or gravity wave, respectively. The greater-than sign reminds us that the Stokes line corresponds to the location where the base solution reaches peak exponential dominance over the capillary or gravity wave (Dingle 1973).

However, in inferring the behaviour of the Stokes contributions as Δ is decreased from $\Delta > 0$ to $\Delta < 0$, we must take great care in selecting the correct branch of the various square roots if we wish to continue to identify the same negative sign in D_{\pm} to gravity waves and the same positive sign to capillary waves. A much easier mechanism is to see *a posteriori* which side the exponentials are decaying or growing and to assign the appropriate wave to the decaying region; we comment on this shortly in §5.3 once we have derived the form of the exponentials. For the moment, however, it is sufficient to claim that as Δ decreases from positive to negative values, the previously coalescent Stokes lines split, with the capillary-associated line moving upstream and the gravity-associated

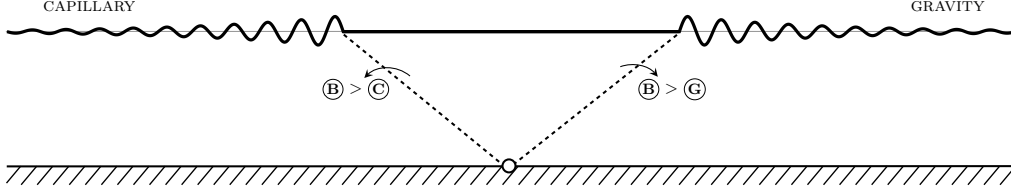


FIGURE 6. In Region II with $\Delta < 0$, the capillary Stokes line moves upstream while the gravity Stokes line moves downstream. We again expect the switching-on of gravity and capillary waves, but because of the non-zero imaginary component of χ , the waves are now exponentially decaying as they tend to infinity.

line moving downstream; this is shown in Figure 6. As the free-surface is analytically continued across these critical lines, we would again expect small waves to switch on, only now the waves decay in the far field.

In the next section, we will explicitly show how the Stokes Phenomenon actually occurs and moreover, we will establish the connection between the resultant waves and the late-order terms of eqns (5.12) and (5.13).

5.2. Stokes smoothing

When an asymptotic expansion is truncated haphazardly, the error is generally algebraically small in ϵ ; in order to observe the smooth switching-on of the waves as the Stokes line is crossed, we must instead truncate the expansions *optimally*, for which the error is exponentially small. In fact, for linear differential equations, seeking this remainder term is equivalent to performing a WKB analysis

To begin, we will truncate the asymptotic expansion in q ,

$$q = \sum_{n=0}^{\mathcal{N}-1} \epsilon^n q_n + R_{\mathcal{N}}. \quad (5.20)$$

Note that the expansions and corresponding expressions for θ are also similarly done, but the fact that $q_n \sim i\theta_n$ from (5.14) allows us to work with only a single variable. Once the truncated sum (5.20) is substituted into eqns (5.5) and (5.6), we get

$$\begin{aligned} \mathcal{L}(R_{\mathcal{N}}; \epsilon) + \epsilon^{\mathcal{N}} \left[\beta \tau i \left(\zeta^2 \frac{d^2 q_{\mathcal{N}-2}}{d\zeta^2} + \zeta \frac{dq_{\mathcal{N}-2}}{d\zeta} \right) - \beta \zeta \frac{dq_{\mathcal{N}-1}}{d\zeta} \right] \\ + \epsilon^{\mathcal{N}+1} \beta \tau i \left[\zeta^2 \frac{d^2 q_{\mathcal{N}-1}}{d\zeta^2} + \zeta \frac{dq_{\mathcal{N}-1}}{d\zeta} \right] = 0, \end{aligned} \quad (5.21)$$

where the linear operator \mathcal{L} is defined by

$$\mathcal{L}(R_{\mathcal{N}}; \epsilon) \equiv \epsilon^2 \beta \tau i \left[\zeta^2 \frac{d^2 R_{\mathcal{N}}}{d\zeta^2} + \zeta \frac{dR_{\mathcal{N}}}{d\zeta} \right] - \epsilon \beta \zeta \frac{dR_{\mathcal{N}}}{d\zeta} - i R_{\mathcal{N}}. \quad (5.22)$$

In (5.21), we can replace the $\mathcal{O}(\epsilon^{\mathcal{N}})$ bracketed quantities with the right-hand side of eqn (5.15), giving

$$\mathcal{L}(R_{\mathcal{N}}; \epsilon) \sim -\epsilon^{\mathcal{N}} \left[i q_{\mathcal{N}} + \epsilon \beta \tau i \left(\zeta^2 \frac{d^2 q_{\mathcal{N}-1}}{d\zeta^2} + \zeta \frac{dq_{\mathcal{N}-1}}{d\zeta} \right) \right]. \quad (5.23)$$

It is easily verified that the solution of the homogeneous equation $\mathcal{L} = 0$ is $R_{\mathcal{N}} = Q e^{-\chi/\epsilon}$

and so to solve the inhomogeneous equation, we let

$$\begin{aligned} R_{\mathcal{N}} &= \mathcal{S} \left[Q e^{-\chi/\epsilon} \right], \\ \frac{dR_{\mathcal{N}}}{d\zeta} &= \mathcal{S} \frac{d}{d\zeta} \left[Q e^{-\chi/\epsilon} \right] + \frac{d\mathcal{S}}{d\zeta} \left[Q e^{-\chi/\epsilon} \right], \\ \frac{d^2 R_{\mathcal{N}}}{d\zeta^2} &= \mathcal{S} \frac{d^2}{d\zeta^2} \left[Q e^{-\chi/\epsilon} \right] + 2 \frac{d\mathcal{S}}{d\zeta} \left[-\frac{d\chi}{d\zeta} Q e^{-\chi/\epsilon} + \frac{dQ}{d\zeta} e^{-\chi/\epsilon} \right] + \frac{d^2 \mathcal{S}}{d\zeta^2} Q e^{-\chi/\epsilon}, \end{aligned}$$

where now \mathcal{S} describes the *Stokes smoothing* parameter, which we expect to smoothly vary from zero to a constant across the Stokes line. When this ansatz for the remainder is substituted into the left hand-side (LHS) of (5.23), we are only left with terms involving derivatives in \mathcal{S} at leading order:

$$\text{LHS of (5.23)} \sim -\epsilon Q e^{-\chi/\epsilon} \left[\beta \zeta + 2\beta \tau i \zeta^2 \frac{d\chi}{d\zeta} \right] \frac{d\mathcal{S}}{d\zeta},$$

and switching to differentiation in χ and using eqn (5.16) to change the bracketed quantities, we then have

$$\text{LHS of (5.23)} \sim -\epsilon Q e^{-\chi/\epsilon} \left[i + \beta \tau i \zeta^2 \left(\frac{d\chi}{d\zeta} \right)^2 \right] \frac{d\mathcal{S}}{d\chi}. \quad (5.24)$$

Since we are interested in the limit that ϵ tends to zero, and so the optimal truncation point, \mathcal{N} , tends to infinity, we can substitute the late-orders ansatz of (5.12) into the right hand-side (RHS) of (5.23), giving

$$\text{RHS of (5.23)} \sim -\frac{\epsilon^{\mathcal{N}} Q \Gamma(\mathcal{N} + \gamma)}{\chi^{\mathcal{N} + \gamma}} \left[i + \beta \tau i \zeta^2 \left(\frac{d\chi}{d\zeta} \right)^2 \left\{ \frac{\epsilon(\mathcal{N} + \gamma + 1)}{\chi} \right\} \right]. \quad (5.25)$$

The optimal truncation point is at $\mathcal{N} \sim \lceil |\chi|/\epsilon \rceil$ (where adjacent terms in the expansion are roughly equal), so we will let $\chi = r e^{i\vartheta}$ and thus set $\mathcal{N} = r/\epsilon + \rho$ where $\rho \in [0, 1)$. Stirling's formula then gives

$$\Gamma(\mathcal{N} + \gamma) = \Gamma(r/\epsilon + \rho + \gamma) \sim \sqrt{2\pi} e^{-r/\epsilon} \left(\frac{r^{\mathcal{N} + \gamma}}{\epsilon^{\mathcal{N}}} \right) \frac{r^{-1/2}}{\epsilon^{\gamma-1/2}}.$$

Changing the derivatives to

$$\frac{d}{d\chi} = -\frac{i e^{-i\vartheta}}{r} \frac{d}{d\vartheta}$$

gives from (5.24) and (5.25),

$$\frac{d\mathcal{S}}{d\vartheta} \left[i + \beta \tau i \zeta^2 \left(\frac{d\chi}{d\zeta} \right)^2 \right] \sim \frac{\sqrt{2\pi r}}{\epsilon^{\gamma+1/2}} \left[i + \beta \tau i \zeta^2 \left(\frac{d\chi}{d\zeta} \right)^2 \frac{1}{e^{i\vartheta}} \right] i (e^{-i\vartheta})^{\frac{r}{\epsilon} + \rho + \gamma} e^{\frac{r}{\epsilon} e^{i\vartheta}} e^{-\frac{r}{\epsilon}} e^{i\vartheta}.$$

The sum of the exponential factors on the right is exponentially small, except near the Stokes line $\vartheta = 0$. The critical scaling occurs with $\vartheta = \sqrt{\epsilon \vartheta}$ and here,

$$\begin{aligned} \exp \left\{ -\frac{r}{\epsilon} \left(1 - \cos \vartheta \right) + i \left(\frac{r \sin \vartheta}{\epsilon} - \vartheta \left(\frac{r}{\epsilon} + \rho + \gamma - 1 \right) + \frac{\pi}{2} \right) \right\} \\ \sim \exp \left\{ -\frac{r \vartheta^2}{2} + \frac{\pi i}{2} + \mathcal{O}(\sqrt{\epsilon}) \right\}. \end{aligned}$$

In total then, we have the local change in the Stokes switching as

$$\frac{dS}{d\bar{\vartheta}} \sim \frac{\sqrt{2\pi}ri}{\epsilon^\gamma} \exp\left(-\frac{r\bar{\vartheta}^2}{2}\right). \quad (5.26)$$

Integrating this expression across the Stokes line from $\bar{\vartheta} = \infty$ (upstream) to $\bar{\vartheta} = -\infty$ (downstream), we find that the jump in the remainder is

$$\left[R_{\mathcal{N}}\right]_{\text{upstream}}^{\text{downstream}} \sim -\frac{2\pi iQ}{\epsilon^\gamma} e^{-\chi/\epsilon} \quad (5.27)$$

and thus across the Stokes line, in a direction from upstream to downstream, the terms

$$q_{\text{exp}}^\pm \sim \frac{4\pi}{\epsilon^\gamma} \Im \left[Q e^{-\chi_\pm/\epsilon} \right], \quad (5.28)$$

$$\theta_{\text{exp}}^\pm \sim \frac{4\pi}{\epsilon^\gamma} \Im \left[\Theta e^{-\chi_\pm/\epsilon} \right], \quad (5.29)$$

are switched on and where, to derive the above expressions, we have added the contribution from analytic continuation into the lower-half plane (or simply, the complex conjugate of the contribution from the upper-half plane). Formulae (5.28) and (5.29) thus provide us with the important connection between the exponentially small waves and the late-order terms (5.12). The apparent jump in the remainder, as given by (5.27), is computed using an error function (5.26); like the concepts of factorial over power divergence and optimal truncation, this smoothed remainder is another ‘universal’ property of singular problems (see Berry 1989*a,b*)

In terms of θ , we will denote the Stokes switching procedure as

$$\begin{aligned} \text{Base series switches-on capillary wave:} & \quad \sum_n \epsilon^n \theta_n \xrightarrow{\textcircled{B} > \textcircled{C}} \sum_n \epsilon^n \theta_n + \theta_{\text{exp}}^+ \\ \text{Base series switches-on gravity wave:} & \quad \sum_n \epsilon^n \theta_n \xrightarrow{\textcircled{B} > \textcircled{C}} \sum_n \epsilon^n \theta_n - \theta_{\text{exp}}^- \end{aligned}$$

either indicating that the base series has switched on a capillary wave, $\textcircled{B} > \textcircled{C}$, or that the base series has switched on a gravity wave, $\textcircled{B} > \textcircled{G}$. Note that because the Stokes smoothing proceeded from $\bar{\vartheta} = -\infty$ to $\bar{\vartheta} = \infty$, across the Stokes line in the direction of downstream-to-upstream, we then add the negation of the jump corresponding to the gravity wave.

We can finally return to our assertion in §5.1 about the selection of the branches of the various square roots and their association to the gravity or capillary waves. We first note from the expression for χ in (5.18) that when $\zeta \in \mathbb{R}^+$,

$$\begin{aligned} \chi_\pm &= \left[\pi \Re(D_\pm) - \Im(D_\pm) \log \zeta \right] + i \left[\pi \Im(D_\pm) + \Re(D_\pm) \log \zeta \right] \\ &= \left[\pi \Re(D_\pm) + \Im(D_\pm) \phi \right] + i \left[\pi \Im(D_\pm) - \Re(D_\pm) \phi \right], \end{aligned} \quad (5.30)$$

using $\log \zeta = -\phi$. Since the waves are given by (5.29), and in particular, their amplitudes are scaled by $e^{-\Re(\chi_\pm)/\epsilon}$, then when $\Delta < 0$, in order for the waves to decay as $\phi \rightarrow \infty$ we need $\Im(D_-) = -\sqrt{\Delta}/(2\tau)$ to be positive. Thus for $\Delta < 0$, we want $\sqrt{\Delta} = -i\sqrt{|\Delta|}$ for gravity waves. A similar argument holds for assigning $\sqrt{\Delta} = i\sqrt{|\Delta|}$ for the case of capillary waves. With these subtle details in mind, we see that the Stokes lines in Figure 6 with χ_+ and χ_- are indeed associated with capillary and gravity waves, respectively.

5.3. Determining Λ and the waves

The final step is to determine the unknown pre-factor $Q = \Lambda$ of eqn (5.28); to do this, we solve for the leading-order solution near the singularity $\zeta = -a$ and match with the late-orders expression of eqn (5.12), which is only valid far away from the singularity.

Near the singularity, a similar argument to the one used in deriving (5.14) can be applied to simplify the problem. From (5.5), we would like to evaluate

$$q_{\text{inner}}(w) - i\theta_{\text{inner}}(w) = \frac{1}{2(\zeta + 1)} + \mathcal{H}[\theta_{\text{outer}}(\zeta)] \quad (5.31)$$

as $\zeta \rightarrow -1$, where the indices help to remind us where the functions q and θ are being evaluated. The left-hand side is evaluated *near* the singularity and thus involves the exact expressions for $q(w)$ and $\theta(w)$ in the inner limit. However, the integrand on the right hand side is integrated over the free-surface, far away from the singularity, thus it involves only the *outer* expansion of $\theta(w)$. But we know that substituting the outer expansion (5.7) into the right-hand side of (5.31) leads to

$$q_{\text{inner}}(w) - i\theta_{\text{inner}}(w) = q_0 + \epsilon \mathcal{H}[\theta_1(\zeta)] + \epsilon^2 \mathcal{H}[\theta_2(\zeta)] + \mathcal{O}(\epsilon^3).$$

Since the integrals are all finite for ζ off the axis, the expansion on the right continues to be well-ordered near the singularity. Thus the leading-order inner solution satisfies

$$q - i\theta \sim \frac{1}{2(\zeta + 1)},$$

so that

$$\begin{aligned} \theta &\sim \frac{i}{2(\zeta + 1)} - iq, \\ \frac{d\theta}{d\zeta} &\sim \frac{-i}{2(\zeta + 1)^2} - i \frac{dq}{d\zeta}, \\ \frac{d^2\theta}{d\zeta^2} &\sim \frac{i}{(\zeta + 1)^3} - i \frac{d^2q}{d\zeta^2}. \end{aligned}$$

Substituting these expressions for θ into (5.6) and simplifying gives

$$\beta\epsilon\zeta \frac{dq}{d\zeta} + \beta\tau\epsilon^2 \left[-i\zeta^2 \frac{d^2q}{d\zeta^2} - i\zeta \frac{dq}{d\zeta} - \frac{i\zeta}{2(\zeta + 1)^2} + \frac{i\zeta^2}{(\zeta + 1)^3} \right] = \frac{i}{2(\zeta + 1)} - iq. \quad (5.32)$$

The scalings for the inner region are given by setting $\epsilon^n q_n \sim q_0$ with (5.7) and (5.12). This gives $\zeta + 1 = i\epsilon\eta$ and $q = -i\bar{q}/(2\epsilon)$ for inner variables η and \bar{q} . Using

$$\frac{d}{d\zeta} = \frac{1}{i\epsilon} \frac{d}{d\eta},$$

and primes to denote differentiation in η , we then have from eqn (5.32):

$$\begin{aligned} \beta\epsilon(-1) \left(\frac{1}{i\epsilon} \right) \left(\frac{-i}{2\epsilon} \right) \bar{q}' + \beta\tau\epsilon^2 \left[-i(-1)^2 \left(\frac{1}{i\epsilon} \right)^2 \left(\frac{-i}{2\epsilon} \right) \bar{q}'' - i(-1) \left(\frac{1}{i\epsilon} \right) \left(\frac{-i}{2\epsilon} \right) \bar{q}' \right. \\ \left. - \frac{i(-1)}{2(i\epsilon\eta)^2} + \frac{i(-1)^2}{(i\epsilon\eta)^3} \right] = \frac{i}{2(i\epsilon\eta)} - i \left(\frac{-i}{2\epsilon} \right) \bar{q}, \end{aligned}$$

and after simplifying, this gives

$$\frac{\beta}{2\epsilon} \bar{q}' + \frac{\beta\tau}{\epsilon} \left[\frac{1}{2} \bar{q}'' - \frac{1}{\eta^3} + \mathcal{O}(\epsilon) \right] = \frac{1}{2\epsilon\eta} - \frac{1}{2\epsilon} \bar{q},$$

so that the equation for the leading-order inner solution is

$$\beta \bar{q}' + \beta \tau \left[\bar{q}'' - \frac{2}{\eta^3} \right] = \frac{1}{\eta} - \bar{q}. \quad (5.33)$$

By examining the form of the outer ansatz (5.12), we expect that in the limit that the inner solution tends to the outer region, it must also diverge like a factorial over power. If we write

$$\bar{q} = \sum_{n=0}^{\infty} \frac{A_n \Gamma(n+1)}{\eta^{n+1}},$$

as $\eta \rightarrow \infty$, this gives from (5.33),

$$-\sum_{n=1}^{\infty} \frac{A_{n-1}(n)\Gamma(n)}{\eta^{n+1}} + \beta \tau \left[\sum_{n=2}^{\infty} \frac{A_{n-2}(n+1)n\Gamma(n+1)}{\eta^{n+1}} - \frac{2}{\eta^3} \right] = \frac{1}{\eta} - \sum_{n=0}^{\infty} \frac{A_n \Gamma(n+1)}{\eta^{n+1}}.$$

In the limit that $\eta \rightarrow \infty$, the first three orders give

$$1 - A_0 = 0 \quad \Rightarrow \quad A_0 = 1, \quad (5.34a)$$

$$-\beta A_0 \Gamma(1) = -A_1 \Gamma(2) \quad \Rightarrow \quad A_1 = \beta, \quad (5.34b)$$

$$-2\beta A_1 + \beta \tau [2A_0 - 2] = -2A_2 \quad \Rightarrow \quad A_2 = \beta^2, \quad (5.34c)$$

while for $n \geq 3$,

$$A_n = \beta (A_{n-1} - \tau A_{n-2}). \quad (5.35)$$

Using D_{\pm} from (4.18), we can show that the solution of the recurrence relation in (5.35) is

$$A_n = \frac{1}{\sqrt{\Delta}} \left\{ \left(\frac{1}{D_-} \right)^n - \left(\frac{1}{D_+} \right)^n \right\} \quad (5.36)$$

with Δ given by (4.19). In order to perform the matching between inner and outer expansions, we first note that

$$\chi_{\pm} = -iD_{\pm} \log(-\zeta) \sim iD_{\pm} (\zeta + 1) = -D_{\pm} \epsilon \eta, \quad (5.37)$$

and then matching is done by applying Van Dyke's (1975) rule. The n^{th} term of the outer solution (n.t.o), written in inner variables and re-expanded to one term (1.t.i) is

$$q \xrightarrow{(n.t.o)} \epsilon^n q_n \sim \frac{\epsilon^n \Lambda \Gamma(n+1)}{\chi^{n+1}} \xrightarrow{(1.t.i)} \frac{(-1)^{n+1} \Lambda \Gamma(n+1)}{\epsilon D_{\pm}^{n+1} \eta^{n+1}} \quad (5.38)$$

where we have used the inner limits of χ from eqn (5.37). Similarly, the leading-order term of the inner region (1.t.i), re-expanded to the n^{th} term in the outer limit (n.t.o) has

$$q \xrightarrow{(1.t.i)} \frac{-i}{2\epsilon} \bar{q} \xrightarrow{(n.t.o)} -\frac{i}{2\epsilon} \frac{A_n \Gamma(n+1)}{\eta^{n+1}},$$

and using the exact solution of the recurrence relation in (5.36) requires

$$\Lambda = \pm \frac{i}{2} \frac{D_{\pm}}{\sqrt{\Delta}}. \quad (5.39)$$

This completes our determination of all the components of the high-order terms of (5.12), as well as the exponentials switched-on across Stokes lines from (5.28)–(5.29).

Indeed, from (5.14), we know that $\Theta = -iQ = -i\Lambda$, and thus from (5.39), we have

$$\Theta = -i\Lambda = \pm \frac{1}{2} \left| \frac{D_{\pm}}{\sqrt{\Delta}} \right| \exp \left[i \left(\text{Arg}(D_{\pm}) - \frac{\text{Arg}(\Delta)}{2} \right) \right]. \quad (5.40)$$

Remembering that we must set $\Im(D_{\pm})\phi = -|\Im(D_{\pm})\phi|$ in order to ensure the proper branch of $\sqrt{\Delta}$ is chosen, we may now combine the components of χ (5.30) and Θ (5.40) into the wave expression for θ_{exp} (5.29) to find that the amplitude of the waves are

$$\text{Amplitude of } \theta_{\text{exp}} \sim \frac{2\pi\bar{\delta}}{\epsilon} \left| \frac{D_{\pm}}{\sqrt{\Delta}} \right| \exp \left[-\frac{\pi\Re(D_{\pm})}{\epsilon} - \frac{|\Im(D_{\pm})\phi|}{\epsilon} \right] \quad (5.41)$$

after having multiplied by $\bar{\delta}$ (since we chose to drop primes following the expansion of (5.4)). A simple flux argument gives $\pi\bar{\delta} = 2\delta$, relating the step height in the physical and potential planes, and so we see that indeed the waves from the standard Fourier analysis (4.22) are the same as the waves from the exponential asymptotics (5.41).

6. Discussion

What is the connection between the treatment of the low-Froude, low-Bond problem using traditional Fourier methods and our new methods in exponential asymptotics?

For both the Fourier method and the exponential asymptotics, the free-surface waves given in (4.22) and (5.41) are produced by deforming a path of integration through the relevant singularities—*explicitly* in Fourier-space for the former, and *implicitly* in the analytically continued domain for latter. We find, however, that when we use exponential asymptotics, concepts like the Stokes Phenomenon and optimal truncation can be clearly interpreted, but if one only sees the problem through Fourier-tinted glasses, then these equivalent notions remain well obfuscated.

Consider the case that $\Delta > 0$. The analysis by exponential asymptotics clearly indicates that the formation of the gravity and capillary waves occurs upon crossing the point $\phi = 0$ on the free-surface, and this is reflected in the integration contour in the Fourier plane, which runs in the upper-half k -plane upstream, but switches into the lower-half k -plane downstream. However, for $\Delta < 0$, the exponential asymptotics clearly show that the capillary and gravity waves only appear on *either side* of the point $\phi = 0$. In particular, this seems to imply that for a small region near $\phi = 0$, the integration contour within Fourier space does not include the complex residue contributions of the four poles—*there are no waves after all!* The connection between the optimal truncation and Stokes smoothing procedure with the standard linearised Fourier theory as $\epsilon \rightarrow 0$ is no longer clear.

How do the infinitude of complex poles in the Fourier plane relate to the optimally truncated asymptotic solution? From (5.10), the low-Froude, low-Bond solution has

$$\theta = -\beta\epsilon\delta \left[\frac{\zeta}{(\zeta + 1)^2} \right] + \mathcal{O}(\epsilon^2). \quad (6.1)$$

This expression must be related to the infinite summation of the residues along the positive or negative imaginary axis of eqn (4.16), which we write as

$$\theta = -\beta\epsilon\delta \sum_{n=0}^{\infty} \left[\frac{\beta_n}{\cos(\pi\beta_n)g'(i\beta_n)} \right] e^{-\beta_n\phi} + \mathcal{O}(e^{-\chi/\epsilon}), \quad (6.2)$$

having multiplied by the size of the step δ . As $\epsilon \rightarrow 0$, the complex roots $\pm i\beta_n$ can be found by setting $\beta_n = n + d$ so that from eqn (4.12) we find

$$d + \frac{1}{3}d^3 + \mathcal{O}(d^5) = \beta^2\epsilon^2(n + d) \left[1 + \beta\tau\epsilon^2(n + d)^2 + \mathcal{O}(\epsilon^4, d^4) \right],$$

and d can be expanded as a (regular) perturbation series in powers of ϵ . Now if we

substitute $\beta_n \sim n$ back into eqn (6.2), we find

$$\theta = -\beta\epsilon\delta \sum_{n=0}^{\infty} (-1)^{n+1} n \zeta^n + \mathcal{O}(\epsilon^2),$$

after making the substitution $\zeta = e^\phi$. In fact, we may truncate this sum at $n = \mathcal{N}$ with

$$\sum_{n=0}^{\mathcal{N}} (-1)^{n+1} n \zeta^n = \left[\frac{\zeta}{(\zeta + 1)^2} \right] \left\{ 1 - (-\zeta)^{\mathcal{N}} + \mathcal{N}(-\zeta)^{\mathcal{N}} + (-1)^{\mathcal{N}} \mathcal{N} \zeta^{\mathcal{N}+1} \right\}.$$

Then selecting $\mathcal{N} \sim \log \epsilon / \log \zeta$, we have

$$\theta = -\beta\epsilon\delta \left[\frac{\zeta}{(\zeta + 1)^2} \right] + \mathcal{O}(\epsilon^2).$$

What we have thus shown is that by adding \mathcal{N} of the residues along the imaginary axis, we can reconstruct the *exact* form of the leading-order term of the asymptotic approximation (6.1) using only the leading order behaviour of β_n . For a general term of the optimally truncated approximation (5.20), we would need to also truncate the expansion of each residue

$$\beta_n = \beta_n^{(0)} + \epsilon \beta_n^{(1)} + \epsilon^2 \beta_n^{(2)} + \dots,$$

and then add up a further truncated sum from eqn (6.2) in order to retrieve the precise form. But because this involves a composite function of many truncated sums, the full process is likely to be excessively complicated. The exponential asymptotics indicates that the region near the center of the free surface should be wave free, and so we conclude that the infinite sum (6.2) must be destructively interfering with the Fourier waves (4.22) when $\phi = \mathcal{O}(1)$.

Ultimately, however, the bridge between Fourier analysis and exponential asymptotics becomes less important as we move on to study the nonlinear problem, where only the latter method is applicable. In the next part (Trinh & Chapman 2013), we will show how exponential asymptotics can be used without first linearising for small obstructions, thus providing an asymptotic approximation valid for $\mathcal{O}(1)$ geometries. There, we shall see that the availability of multiple singularities in the geometry, coupled with the interplay of gravitational and cohesive effects, leads to the discovery of a remarkable set of new gravity-capillary waves.

Appendix A. Linear classification of solutions

For the finite-depth flow in a channel of height π , the dispersion relation and its derivative can be written as

$$g(k) = kF^2 - \tanh(\pi k)(Bk^2 + 1), \quad (\text{A } 1)$$

$$g'(k) = F^2 - \text{sech}^2(\pi k)(Bk^2 + 1) - \tanh(\pi k)(2kB). \quad (\text{A } 2)$$

The nature of the zeros of the dispersion relation provide a classification of the linearised solutions in the (F, B) plane. For all values of F and B , $k = 0$ is a root of (A 1), but it plays no role unless $F = 1$. There are an infinite number of purely imaginary roots at $k = \pm i\beta_0, \pm i\beta_1, \dots$. The relevant regions in the linear classification are shown in Figure 7.

First, consider Region I of the (F, B) plane. Here, the dispersion relation has four real roots: $k = \pm k_0$ and $k = \pm k_1$ where $0 < k_0 < k_1$; clearly, k_0 corresponds to the gravity waves and k_1 to the capillary waves. Physically, we would expect capillary waves

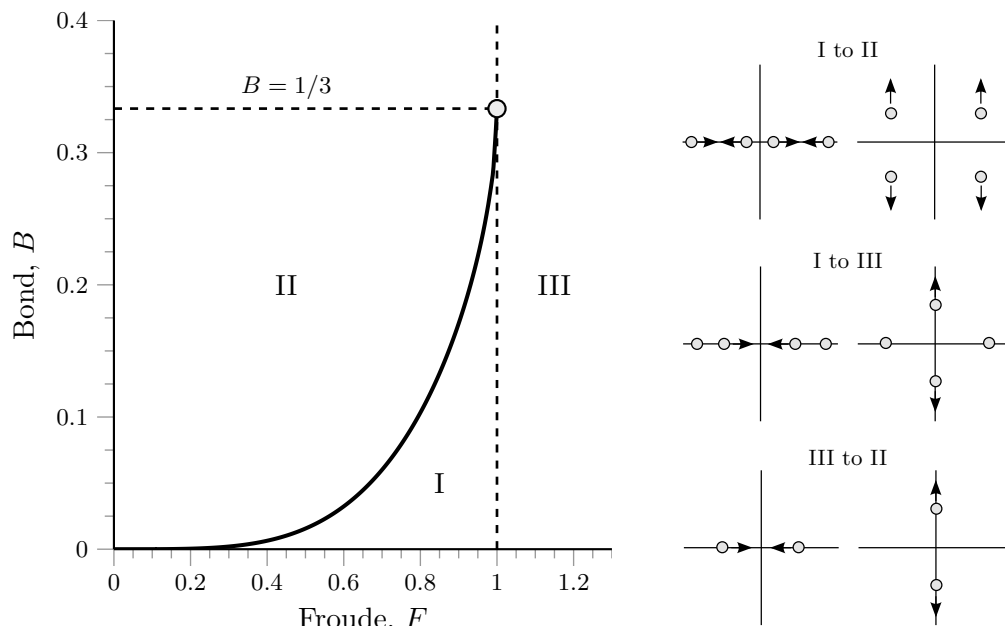


FIGURE 7. The three regions in (F, B) space which distinguish the linearised solutions are shown on the left. The transitions between the different regions can be understood by following the movements of the four (possibly repeated) wavenumbers in the complex k -plane, shown on the right.

upstream and gravity waves downstream, and this subcritical region is the one relevant to Rayleigh's (1883) fishing-pole problem.

As $B \rightarrow 0$, $\pm k_1 \rightarrow \pm\infty$ and only the gravity waves remain. Alternatively, if we hold F fixed and increase B , then the roots coalesce at a critical value (corresponding to the dispersion curve $F = F_m$) and for B still larger, they split, forming four complex roots; here, we would expect localised solitary solutions. Physically, this bifurcation point corresponds to point where the group velocity of the wave equals the phase velocity, so that $k_0 = k_1 = k^*$ and critical dispersion curve $F = F_m$ is then defined by solving $g(k^*) = g'(k^*) = 0$.

Next, suppose we begin again in Region I, hold B fixed, and increase F . Then we find that the two gravity roots coalesce at the origin, and then split, moving upwards and downwards on the imaginary axis. This bifurcation describes the more complex phenomena of the exponentially radiating waves of the fifth-order Korteweg-de Vries eqn.

Finally, if we begin in Region III with $B > 1/3$, and hold B fixed whilst decreasing F , we transition back to Region II. This corresponds to having the two capillary roots coalescing near the origin, and then splitting onto the imaginary axis.

REFERENCES

- AKYLAS, T. R. & GRIMSHAW, R. H. J. 1992 Solitary internal waves with oscillatory tails. *J. Fluid Mech.* **242**, 279–298.
- BEALE, J. T. 1991 Exact solitary water waves with capillary ripples at infinity. *Comm. Pure Appl. Math.* **44**, 211–257.
- BERRY, M. V. 1989a Stokes' phenomenon; smoothing a Victorian discontinuity. *Publ. Math. of the Institut des Hautes Études scientifiques* **68**, 211–221.

- BERRY, M. V. 1989*b* Uniform asymptotic smoothing of Stokes discontinuities. *Proc. Roy. Soc. London A* **422**, 7–21.
- BOYD, J. P. 1998 *Weakly nonlocal solitary waves and beyond-all-orders asymptotics*. Kluwer Academic Publishers.
- BOYD, J. P. 1999 The Devil's invention: Asymptotics, superasymptotics and hyperasymptotics. *Acta Applicandae* **56**, 1–98.
- CHAPMAN, S. J., KING, J. R. & ADAMS, K. L. 1998 Exponential asymptotics and Stokes lines in nonlinear ordinary differential equations. *Proc. R. Soc. Lond. A* **454**, 2733–2755.
- CHAPMAN, S. J. & MORTIMER, D. B. 2005 Exponential asymptotics and Stokes lines in a partial differential equation. *Proc. R. Soc. A* **461** (2060), 2385–2421.
- CHAPMAN, S. J. & VANDEN-BROECK, J.-M. 2002 Exponential asymptotics and capillary waves. *SIAM J. Appl. Math.* **62** (6), 1872–1898.
- CHAPMAN, S. J. & VANDEN-BROECK, J.-M. 2006 Exponential asymptotics and gravity waves. *J. Fluid Mech.* **567**, 299–326.
- COSTIN, O. 2008 *Asymptotics and Borel summability*, , vol. 141. Chapman & Hall/CRC.
- CRAPPER, G. D. 1957 An exact solution for progressive capillary waves of arbitrary amplitude. *J. Fluid Mech.* **2** (6), 532–540.
- DEBNATH, LOKENATH 1994 *Nonlinear Water Waves*. Academic Press.
- DIAS, F., MENASCE, D. & VANDEN-BROECK, J.-M. 1996 Numerical study of capillary-gravity solitary waves. *Eur. J. Mech. B/Fluids* **15** (1), 17–36.
- DIAS, F. & VANDEN-BROECK, J.-M. 1993 Nonlinear bow flows with spray. *J. Fluid Mech.* **255**, 91–102.
- DINGLE, R. B. 1973 *Asymptotic Expansions: Their Derivation and Interpretation*. Academic Press, London.
- FORBES, L. K. 1983 Free-surface flow over a semi-circular obstruction, including the influence of gravity and surface tension. *J. Fluid Mech.* **127**, 283–297.
- GRANDISON, S. & VANDEN-BROECK, J.-M. 2006 Truncation approximations for gravity-capillary free-surface flows. *J. Eng. Math.* **54**, 89–97.
- GRIMSHAW, R. 2010 *Asymptotic Methods in Fluid Mechanics: Survey and Recent Advances*, chap. Exponential Asymptotics and Generalized Solitary Waves, pp. 71–120. SpringerWienNewYork.
- HUNTER, J. K. & SCHEURLE, J. 1988 Existence of perturbed solitary wave solutions to a model equation for water waves. *Physica D* **32**, 253–268.
- HUNTER, J. K. & VANDEN-BROECK, J.-M. 1983 Solitary and periodic gravity-capillary waves of finite amplitude. *J. Fluid Mech.* **134**, 205–219.
- KING, A. C. & BLOOR, M. I. G. 1987 Free-surface flow over a step. *J. Fluid. Mech.* **182**, 193–208.
- KING, A. C. & BLOOR, M. I. G. 1990 Free-surface flow of a stream obstructed by an arbitrary bed topography. *Q. J. Mech. appl. Math.* **43**, 87–106.
- LAMB, H. 1932 *Hydrodynamics*. Dover Publications.
- LUSTRI, C. J., MCCUE, S. W. & BINDER, B. J. 2012 Free surface flow past topography: A beyond-all-orders approach. *Eur. J. Appl. Math.* **1** (1), 1–27.
- MALEEWONG, M., ASAVANANT, J. & GRIMSHAW, R. 2005*a* Free surface flow under gravity and surface tension due to an applied pressure distribution: I Bond number greater than one-third. *Theor. Comput. Fluid Dyn.* **19** (4), 237–252.
- MALEEWONG, M., ASAVANANT, J. & GRIMSHAW, R. 2005*b* Free surface flow under gravity and surface tension due to an applied pressure distribution: II Bond number less than one-third. *Eur. J. Mech. B/Fluids* **24**, 502–521.
- MORTIMER, D. B. 2004 Exponential asymptotics and stokes lines in partial differential equations. PhD thesis, University of Oxford.
- OGILVIE, T. F. 1968 Wave resistance: The low speed limit. *Tech. Rep.*. Michigan University, Ann Arbor.
- OLDE DAALHUIS, A. B. 1999 On the computation of Stokes multipliers via hyperasymptotics. Resurgent functions and convolution integral equations. *Surikaiseikikenkyusho Kokyuroku* (1088), 68–78.
- OLDE DAALHUIS, A. B., CHAPMAN, S. J., KING, J. R., OCKENDON, J. R. & TEW, R. H. 1995

- Stokes Phenomenon and matched asymptotic expansions. *SIAM J. Appl. Math.* **55**(6), 1469–1483.
- POMEAU, Y., RAMANI, A. & GRAMMATICOS, B. 1988 Structural stability of the Korteweg-de Vries solitons under a singular perturbation. *Physica D* **31**, 127–134.
- LORD RAYLEIGH 1883 The form of standing waves on the surface of running water. *Proc. Lond. Math. Soc.* **15**, 69–78.
- RUSSELL, J. S. 1844 Report on waves. In *14th meeting of the British Association for the Advancement of Science* (ed. John Murray), pp. 311–390. London.
- SCHOOLEY, A. H. 1960 Double, triple, and higher-order dimples in the profiles of wind-generated water waves in the capillary-gravity transition region. *J. Geophys. Res.* **65**, 4075–4079.
- STOKER, J. J. 1957 *Water waves*. Interscience Publishers, Inc.
- SUN, S. M. 1991 Existence of a generalized solitary wave solution for water with positive bond number less than $1/3$. *J. Math. Anal. Appl.* **156**, 471–504.
- THOMSON, SIR WILLIAM (BARON KELVIN) 1871 Hydrokinetic solutions and observations. *Phil. Mag.* **42** (4), 374.
- TRINH, P. H. 2010 *Asymptotic Methods in Fluid Mechanics: Survey and Recent Advances*, chap. Exponential Asymptotics and Stokes Line Smoothing for Generalized Solitary Waves, pp. 121–126. SpringerWienNewYork.
- TRINH, P. H. & CHAPMAN, S. J. 2013 New gravity-capillary waves at low speeds. Part 2: Nonlinear theory. *Submitted to J. Fluid Mech.* —.
- TRINH, P. H., CHAPMAN, S. J. & VANDEN-BROECK, J.-M. 2011 Do waveless ships exist? Results for single-cornered hulls. *J. Fluid Mech.* **685**, 413–439.
- TUCK, E. O. 1991 Ship-hydrodynamic free-surface problems without waves. *J. Ship Res.* **35** (4), 277–287.
- VAN DYKE, M. 1975 *Perturbation Methods in Fluid Mechanics: By Milton Van Dyke. Annotated Ed.* Parabolic Press.
- VANDEN-BROECK, J.-M. 2002 Wilton ripples generated by a moving pressure distribution. *J. Fluid Mech.* **451**, 193–201.
- VANDEN-BROECK, J.-M. & DIAS, F. 1992 Gravity-capillary solitary waves in water of infinite depth and related free-surface flows. *J. Fluid Mech.* **240**, 549–557.
- WILTON, J. R. 1915 On ripples. *Phil. Mag.* **29**, 688–700.
- XIE, X. & TANVEER, S. 2003 Rigorous results in steady finger selection in viscous fingering. *Archive for Rational Mechanics and Analysis* **166** (3), 219–286.

